ARTICLES

Electronic structure of $NiS_{1-x}Se_x$

S. R. Krishnakumar, N. Shanthi, Priya Mahadevan and D. D. Sarma*
Solid State and Structural Chemistry Unit, Indian Institute of Science, Bangalore 560012, India
(Received 7 October 1999; revised manuscript received 31 January 2000)

We investigate the electronic structure of the metallic $NiS_{1-x}Se_x$ system using various electron spectroscopic techniques. The band-structure results do not describe the details of the spectral features in the experimental spectrum, even for this paramagnetic metallic phase. However, a parametrized many-body multiband model is found to be successful in describing the Ni $2p$ core level and valence band, within the same model. The asymmetric line shape as well as the weak intensity feature in the Ni $2p$ core-level spectrum have been ascribed to extrinsic loss processes in the system. The presence of satellite features in the valence-band spectrum shows the existence of the lower Hubbard band, deep inside the pd metallic regime, consistent with the predictions of the dynamical mean-field theory.

I. INTRODUCTION

Electronic structure of $3d$-transition metal compounds has been an active area of research for many decades, owing to their rich and diverse physical properties, often exhibiting exotic transport and magnetic properties. In particular, the electronic structure of the hexagonal nickel sulphide (NiS) has attracted a lot of interest[1,2] due to the fact that it has a first-order phase transition as a function of temperature at about 260 K. The high-temperature phase is a Pauli paramagnetic metal, transforming isostructurally to an antiferromagnetic state with nearly temperature-independent resistivity.[3,4] The high-temperature phase is metallic with a resistivity in the order of 10^{-5} Ω cm,[3,4] which is comparable with other highly metallic inorganic compounds of $3d$-transition elements.[5] The metallic state can be stabilized by the application of pressure or substitution with Se for S. A pressure of more than 20 kbar (Ref. 6) or a Se percentage of more than 13% (Ref. 7) suppresses the electronic phase transition, stabilizing the metallic phase down to the lowest temperature. At room temperature, the hexagonal NiS crystallizes in the NiAs structure having space group $P6_3/mmc$ (D_{6h}^4) and lattice parameters, $a=3.440$ Å and $c=5.351$ Å.[8] The Ni^{2+} is in an octahedral environment of sulphur atoms in NiS and these NiS_6 octahedra are edge shared within the ab plane and face shared along the c axis, forming a three-dimensional network of Ni-S connectivity in this system.

In spite of its interesting properties, there have been few studies to understand the electronic structure of these compounds. Band-structure calculations[9–11] indeed yield a metallic ground state for the high-temperature phase. However, the details of the electronic structure, as shown in this paper, cannot be entirely described within the band theory due to the presence of substantial correlation effects even in the metallic phase. Different configuration interaction models have been employed in order to explain the valence band[12] and the transition-metal core-level spectra;[13] however, there has not been any attempt to describe both using a single model and with a single set of parameters. In this paper, we investigate the electronic structure of the metallic $NiS_{1-x}Se_x$ system using x-ray photoemission (XP), ultraviolet photoemission (UP), and bremsstrahlung isochromat (BI) spectroscopic measurements in conjunction with *ab initio* band-structure calculations as well as parametrized many-body calculations, in order to provide a consistent and quantitative description of the electronic structure and the electronic parameter strengths controlling the physical properties of this system.

II. EXPERIMENTAL

Polycrystalline samples of $NiS_{1-x}Se_x$ with $x=0.0$ and 0.15 used for this paper were prepared following the standard solid-state reaction techniques reported in the literature;[1,7] x-ray diffraction patterns as well as resistivities of the samples were found to be in agreement with the reported data in the literature.[7,8] Spectroscopic measurements were carried out in a combined VSW spectrometer with a base pressure of 2×10^{-10} mbar equipped with a monochromatized Al $K\alpha$ x-ray source, He-discharge lamp, and an electron gun. XP, BI, and UP spectroscopic measurements were performed on the samples with an overall instrumental resolution of better than 0.8 eV, 0.8 eV, and 90 meV, respectively. BI spectra have been recorded by monochromatizing the emitted photons at 1486.6 eV. The sample surface was cleaned *in situ* periodically during the experiments by scraping with an alumina file and the surface cleanliness was monitored by recording the carbon $1s$ and oxygen $1s$ XP signals. The reproducibility of the spectral features was confirmed in each case. The binding energy was calibrated to the instrumental Fermi level that was determined by recording the Fermi-edge region from a clean silver sample. Experimental spectra of NiS reported here were collected for the highly conducting state at room temperature ($\sim$295 K), while those of $NiS_{0.85}Se_{0.15}$, which does not exhibit any transition, were collected at $\sim$120 K. Using high-resolution photoemission spectroscopy, it has been established[1] that the electronic structure close to E_F changes across the electronic

transition at ~260 K. However, our low-resolution spectroscopic results show hardly any change in the spectra across the transition either in the valence band or in the core levels, in agreement with previous studies,[12,14] establishing similar gross electronic structures with comparable electronic parameter strengths for both phases across the electronic transition.

Scalar relativistic linearized muffin-tin orbital (LMTO) band-structure calculations have been performed within the atomic sphere approximation for the paramagnetic phase of NiS with the real crystal structure. The unit cell has two formula units and the sphere radii for Ni and S were 2.4 and 3.12 a.u., respectively. In this calculation, convergence was obtained self-consistently using *s*, *p*, and *d* basis at each atomic sphere with 186 *k* points in the irreducible part of the Brillouin zone. In order to understand and compare the experimental electronic structure with that obtained from the band-structure calculations, it is necessary to include the effects of photoemission cross sections of various levels. Thus, the theoretical spectra based on the band-structure calculations were constructed by multiplying the various partial density-of-states (DOS) with the corresponding cross sections computed within the formalism of Ref. 15. The cross section weighted DOS was then convoluted with a Lorentzian with energy dependent full width at half maximum, to account for the lifetime broadening and a Gaussian to describe the instrumental resolution broadening.

Core-level and valence-band (VB) spectra were calculated for a NiS_6 cluster with the geometry in accordance with the bulk crystal structure of this compound, within a parametrized many-body multiband model including orbital dependent electron-electron (multiplet) interactions.[16,17] The multiplet interactions within the $3d$ manifold were expressed in terms of the Slater integrals F^0_{dd}, F^2_{dd}, and F^4_{dd} and those within the $2p$-$3d$ manifold were expressed in terms of F^0_{pd}, F^2_{pd}, G^1_{pd}, and G^3_{pd}. The values F^2_{dd} (=9.79 eV), F^4_{dd} (=6.08 eV), F^2_{pd} (=6.68 eV), G^1_{pd} (=5.07 eV), and G^3_{pd} (=2.88 eV) were taken to be 80% of the Ni atomic Hartree-Fock values. The monopole terms, F^0_{dd} and F^0_{pd} were treated as parameters and therefore, varied to fit the experimental spectrum. It is often more convenient to discuss the electron-electron interaction strengths in terms of the multiplet averaged quantities, U_{dd} and U_{pd}, where

$$U_{dd}=F^0_{dd}-\frac{2}{63}(F^2_{dd}+F^4_{dd}), \tag{1}$$

$$U_{pd}=F^0_{pd}-\frac{1}{15}G^1_{pd}-\frac{3}{70}G^3_{pd}. \tag{2}$$

The multiplet averaged U_{pd} term was set to have a value 1.2 times that of U_{dd},[17] thus reducing the number of freely adjustable parameters in the model. The hopping interaction strengths between Ni $3d$ and S $3p$ were expressed in terms of the Slater-Koster parameters $(pd\sigma)$ and $(pd\pi)$ and that between the different bonding S $3p$ orbitals were expressed in terms of $(pp\sigma)$ and $(pp\pi)$.[18] We fixed the ratio between $(pd\pi)$ and $(pd\sigma)$ to be -0.5, while that between $(pp\pi)$ and $(pp\sigma)$ to be -0.2, in these calculations.

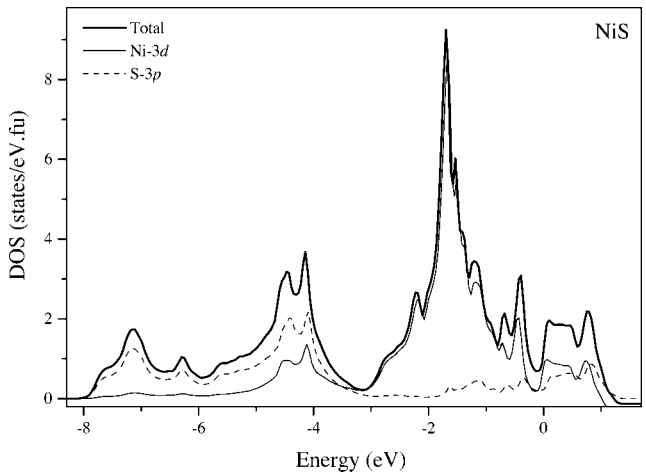

FIG. 1. DOS of NiS from the band-structure calculation for the paramagnetic state. The thick-solid line represents the total DOS. The thin-solid and dashed lines are the Ni $3d$ and S $3p$ partial DOS, respectively.

The calculations were performed in the symmetry adapted (t_{2g} and e_g) basis including the transition-metal $3d$ and the bonding sulphur $3p$ orbitals. In the calculation for the valence-band spectrum, the S $3p$ spectral contribution was also calculated within the same parametrization. As the size of the Hamiltonian is large, the Lanczos method was used to evaluate the spectral function and the calculated one-electron removal spectra were appropriately broadened to simulate the experimental spectra. In the Ni $2p$ core-level calculation, Doniach-Sunjic line shape function was used for broadening the discrete energy spectrum of the cluster model, in order to represent the asymmetric line shape of core levels from these highly metallic compounds, consistent with other core levels in the system. In the case of VB calculations, an energy dependent Lorentzian function was used for the lifetime broadening. Other broadening effects such as the resolution broadening and solid-state effects were taken into account by convoluting the spectra with a Gaussian function. The broadening parameters were found to be consistent with values used for similar systems.[17] Taking into account the different atomic cross sections for the Ni $3d$ and S $3p$ states, it is necessary to calculate a weighted average of these two contributions to the valence band. The atomic cross section ratio[19] between S $3p$ and Ni $3d$ states (≈ 0.17) is not appropriate in this context, since solid-state effects alter this ratio significantly. It was found that the S $3p$/Ni $3d$ cross section ratio of approximately 5.5 times that obtained from the atomic calculations gives the best result for the cluster calculations.

III. RESULTS AND DISCUSSIONS

The total DOS for NiS along with the Ni *d* and S *p* partial DOS obtained from the band-structure calculations for the paramagnetic phase are shown in Fig. 1. The calculated DOS is in good agreement with previous reports.[10,11] The Fermi level lies close to a minimum in the DOS, and there is a finite DOS at the E_F, consistent with the metallic nature of the system. The total DOS between -3 and 1 eV is dominated by Ni *d* contributions with the energy region around

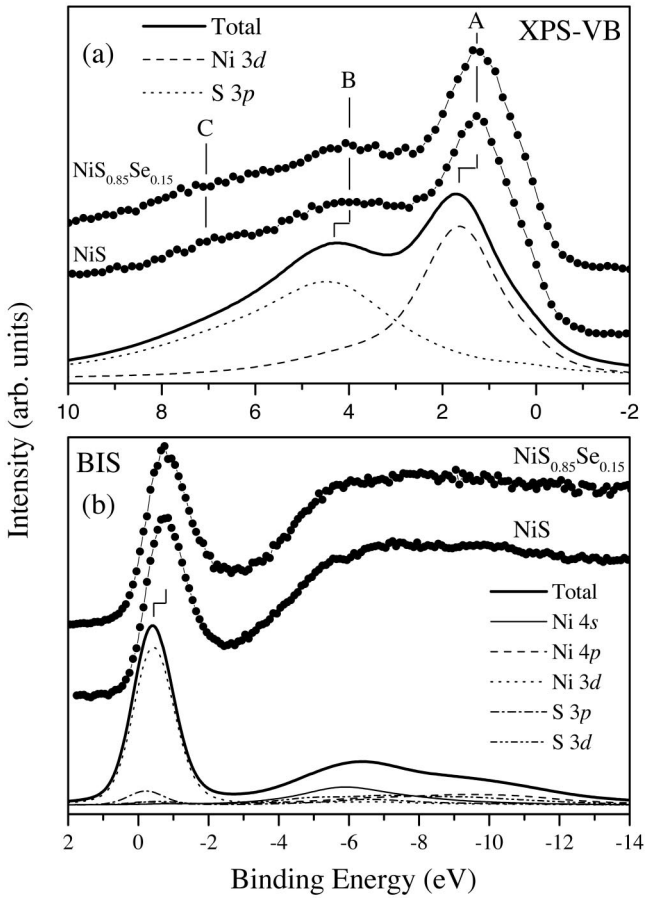

FIG. 2. (a) Experimental valence-band spectra using Al Kα for NiS and $NiS_{0.85}Se_{0.15}$ along with the calculated spectrum obtained from band-structure calculations. The thick-solid line represents the total spectrum, while the thin-solid and dashed lines correspond to the contributions to the calculated spectrum from Ni $3d$ and S $3p$ partial DOS, respectively. (b) Experimental BI spectra for NiS and $NiS_{0.85}Se_{0.15}$ along with calculated spectrum obtained from the band-structure calculations. Various contributions to the total spectrum are represented by different line types.

the most intense peak in the DOS at about -1.65 eV dominated by the Ni t_{2g} states and the features at higher energies ($\geqslant -1$ eV) arising primarily from the e_g states. As a consequence of the high covalency of the system, the Ni $3d$ (e_g) states have substantial contribution from S $3p$ states. These states constitute the antibonding states due to Ni d-S p interactions. Their bonding counterparts are located between -5 and -3 eV and have dominant S $3p$ contributions. The nonbonding states of the system, centered around -7 eV, is weaker in intensity and is stabilized at a higher binding energy compared to Ni d-S p bonding states, which is a generic feature as seen in the case of the transition-metal monosulphides.[11]

We compare the experimental XP valence-band and BI spectra corresponding to the occupied and unoccupied parts of the electronic structures for NiS and $NiS_{0.85}Se_{0.15}$ in Figs. 2(a) and 2(b), respectively. The calculated spectra for NiS, obtained using various partial DOS as explained in the previous section, are also shown for comparison. The XP and BI spectra of NiS and $NiS_{0.85}Se_{0.15}$ show finite spectral intensity at E_F, indicating their highly metallic conductivity. It is clear from the experimental spectra in Figs. 2(a) and 2(b) that the substitution of Se in place of S does not cause any perceptible change in the XP valence-band spectra as well as in the BI spectra. This indicates that the occupied as well as the unoccupied parts of the electronic structure in these two compounds are similar, in agreement with the similar magnetic and transport properties of the two compounds.

Figure 2(a) shows that the peak in the experimental spectra around 1.3-eV binding energy (marked A) essentially consists of Ni $3d$ states, while that at $\sim$4-eV binding energy (marked B) is due to the S $3p$ contribution. However, the calculated spectrum does not describe the experimental spectra accurately, as the energy positions of the different features, A and B are not correctly predicted by the calculation, but are shifted to higher binding energies compared to the experiment. Additionally, the experimental feature A is narrower compared to the calculated one. Moreover, the structure around the 7-eV binding energy (marked C) in the experimental spectra is absent in the theoretical spectrum. In the unoccupied part of the electronic structure, the peak at around -0.7 eV in the experimental BI spectra is contributed mainly by the unoccupied e_g states of the Ni $3d$ manifold, strongly hybridized with the S $3p$ bands, as seen from Fig. 1. The strong suppression in the S $3p$ contribution in the calculated spectrum [Fig. 2(b)] compared to the partial DOS (Fig. 1) in the vicinity of E_F arises from a substantially lower photoemission cross section for the S $3p$ states compared to Ni $3d$ at Al Kα x-ray energies. The broad spectral features above 4 eV are due to the various high-energy unoccupied states in the system, such as Ni $4s,4p$, and S $3d$. Similar to the case in XP spectra, the band-structure calculation, while providing a reasonable description of the overall spectral features observed in the BI spectra, fails to reproduce the energy position of the feature A in Fig. 2(b) by approximately 0.3 eV. These failures of the band theory to explain the electronic structure of this system indicate that electron correlation effects are important even in the paramagnetic metallic phase.

The valence band spectra of NiS and $NiS_{0.85}Se_{0.15}$ recorded using different photon energies, namely, 1486.6 eV (XPS), 40.8 eV (He II), and 21.2 eV (He I) are compared in Fig. 3. The various features are marked as A, B, and C and represent the same features as in Fig. 2(a). At all the photon energies, there is a finite spectral intensity at E_F. Besides providing a much higher resolution compared to the XPS, UP spectra with He I and II radiations allow for a wider variation in the relative photoemission cross sections of Ni $3d$ and S $3p$, leading to an easy identification of their relative contributions to the valence-band spectra. The marked loss in the intensity of the feature B for a moderate increase of the photon energy between (He I) and (He II) radiations arises from the Cooper minimum in the S $3p$ photoionization cross section at around 50 eV, clearly establishing the dominance of S $3p$ contributions in the energy range of the feature B, with feature A having predominantly Ni $3d$ contributions, in agreement with previous works.[12] The valence-band spectra for NiS and $NiS_{0.85}Se_{0.15}$ taken at various photon energies are very similar, showing the similarity in their electronic structure within the solid solution $NiS_{1-x}Se_x$ for $x \leqslant 0.15$.

The transition-metal $2p$ core-level spectra in transition-

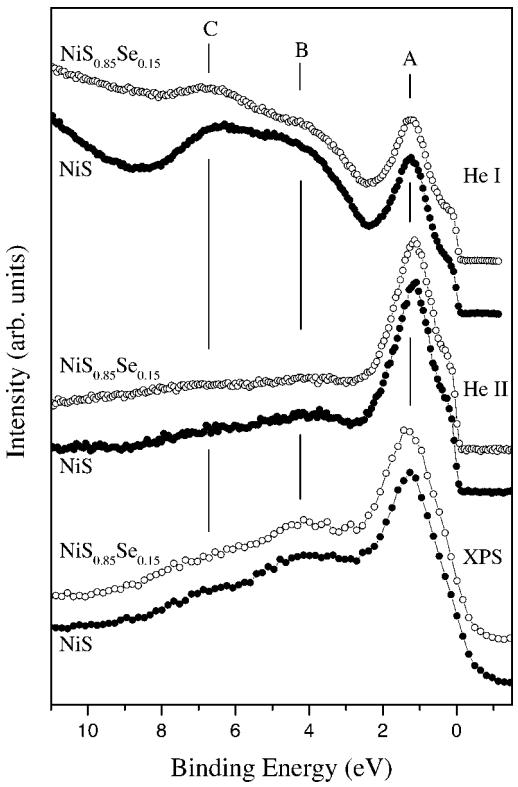

FIG. 3. Experimental valence-band spectra for NiS and $NiS_{0.85}Se_{0.15}$ using 1486.6-eV (XPS), 40.81-eV (He II), and 21.2-eV (He I) photon energies. Various features in the spectra are shown by the vertical lines and are labeled as A, B, and C (see text).

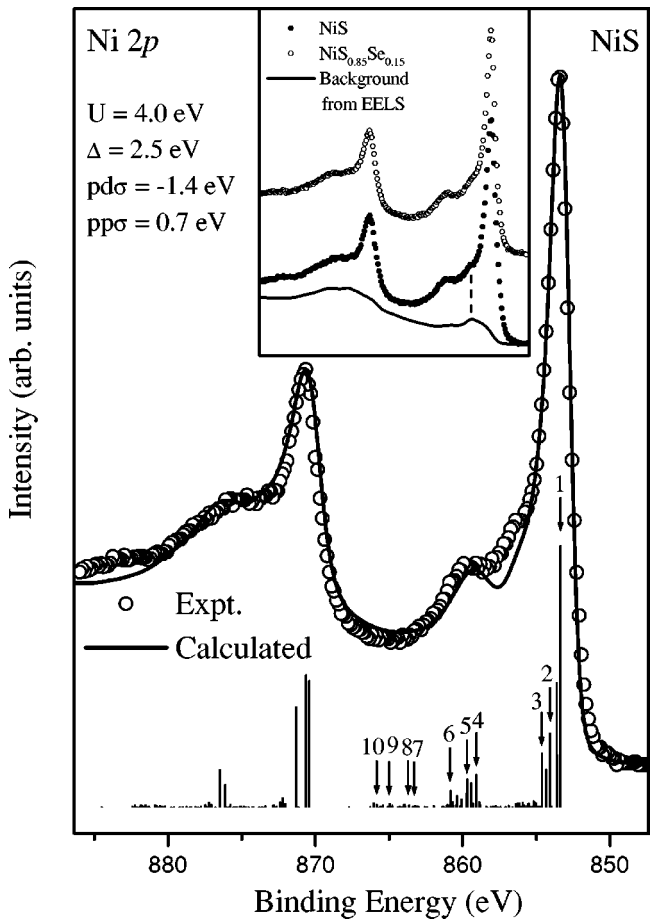

FIG. 4. Experimental Ni $2p$ spectrum (open circles) along with the calculated spectrum (solid line) for NiS obtained from the cluster calculation. Various final states of the cluster calculation and the corresponding intensity contributions without any broadening are shown as the bar diagram. Inset shows Ni $2p$ core-level spectra for NiS and $NiS_{0.85}Se_{0.15}$ along with the inelastic-scattering background function obtained from EELS for NiS. The dashed-vertical line shows the structure in the background function responsible for the feature in the core-level spectra around 856 eV.

metal compounds often reveal important information on their electronic structures. The Ni $2p$ core-level spectra for NiS and $NiS_{0.85}Se_{0.15}$ are shown in the inset of Fig. 4; the two spectra are very similar to each other. Each spectrum consists of a spin-orbit split, $2p_{3/2}$ and $2p_{1/2}$ peaks at 853.4-eV and 870.7-eV binding energies, respectively, with pronounced satellite features at 860 eV and 876 eV, suggesting that electron correlations are important in the system. The satellite intensity relative to the main peak is considerably more in the $2p_{1/2}$ region compared to that in the $2p_{3/2}$ region. While it is indeed possible to have different shapes and intensities for the two satellite features accompanying $2p_{3/2}$ and $2p_{1/2}$ features due to details of the multiplet interactions, such a strong variation between the two satellites as observed here is unexpected. In order to explore the possibility of strong variations in the inelastic background function, normally assumed to vary smoothly, we have performed electron-energy-loss spectroscopy (EELS) on these samples, with the same primary energy as that of the Ni $2p$ core-level peak. The inelastic loss background appropriate for the Ni $2p$ photoemission spectrum was constructed from the experimental EELS spectrum by convoluting it with a Gaussian to obtain similar width for the elastic peak as that in the core-level main peak. The region near the elastic peak was replaced by an integral background function. The total inelastic background was then generated by adding the loss functions corresponding to the $2p_{3/2}$ and $2p_{1/2}$ features with the intensities given by the degeneracy ratio (2:1) of the core levels. The resulting background function is shown in the inset of Fig. 4 as a solid line. We find that there is an intense and structured contribution to the background function arising from a plasmon band overlapping the $2p_{1/2}$ satellite region and resulting in the anomalously large satellite intensity in the $2p_{1/2}$ region compared to that in the $2p_{3/2}$ region. It is also seen that at around 856 eV, there is a peaklike structure in the inelastic background; this appears at the same position as that of a weak intensity feature at about the same energy in the core-level experimental spectrum as shown by the vertical-dashed line in the inset of Fig. 4. This structure in the inelastic-scattering background could have its origin from the interband p-d transitions. Thus, it appears that this weak intensity shoulder in the experimental Ni $2p$ spectrum is largely due to this extrinsic loss feature in the background function. Our explanation is contrary to the earlier interpretation[13] of this feature as arising from intrinsic processes.

In order to obtain a quantitative description of the electronic structure of this system, we have calculated the Ni $2p$ core-level and VB spectra within a single model involving a NiS_6 cluster, retaining the local geometry of the real solid. The calculated Ni $2p$ spectrum (solid line) for the parameter set S-Ni $(pd\sigma) = -1.4$ eV, S-S $(pp\sigma) = 0.7$ eV, Δ

TABLE I. Contributions from various configurations in the final states of the Ni $2p$ core-level photoemission in NiS. The peak numberings correspond to the labels indicated in Fig. 4; the corresponding binding energies (BE) in eV are also shown.

Peak no.	1	2	3	4	5	6	7	8	9	10
BE	853.4	854.1	854.7	859.1	859.7	860.9	863.3	863.7	865.0	865.9
d^8	23.62	12.83	10.77	42.47	25.62	32.90	17.43	16.80	52.44	63.44
$d^9\boldsymbol{L}^1$	57.51	61.87	61.02	24.39	50.86	17.87	37.93	35.80	34.74	28.42
$d^{10}\boldsymbol{L}^2$	18.87	25.30	28.21	33.14	23.52	49.23	44.65	47.40	12.82	8.14

$=2.5$ eV, and $U_{dd}=4.0$ eV, including the experimentally determined inelastic background, is superposed on the experimental spectrum (open circles) in the main panel of Fig. 4, exhibiting a good agreement; the calculated spectrum without any broadening is presented as bar diagrams. There is an underestimation of the intensity around the shoulder to the main peak near 857 eV and around 883-eV binding energies. These small discrepancies are possibly due to the differences between the experimental EELS spectrum used for generating the background function and the actual inelastic loss background for the photoemission spectrum. The previous estimates[13] of the various parameter strengths in NiS obtained from a model that included a fictitious conduction band in addition to Ni $3d$-S $3p$ basis within the cluster model used for the core-level calculation, are $(pd\sigma)=-1.47$ eV, $\Delta=2.5$ eV, and $U_{dd}=5.5$ eV. Thus, the present estimates differ significantly only for U_{dd}, for which we have obtained a smaller value.

The $(pd\sigma)$ values estimated for NiS is similar to that estimated for other divalent nickel sulphides, for example, $(pd\sigma)=-1.5$ eV for NiS_2 and $BaNiS_2$,[20] and for trivalent Ni oxide systems, such as $LaNiO_3$ [$(pd\sigma)=-1.57$ eV (Ref. 21)]. However, divalent Ni oxide systems, such as NiO, typically exhibit a Ni $3d$-O $2p$ $(pd\sigma)=-1.25$ eV.[17] This decrease in the strength of $(pd\sigma)$ for the divalent oxides compared to trivalent ones is due to an increase in the Ni-O distances in the divalent oxides. The similarity in the $(pd\sigma)$ of nickel sulphides and the trivalent Ni oxides, in spite of the differences in their Ni-ligand bond length ($d_{\text{Ni-O}}\simeq 1.93$ Å for $LaNiO_3$ compared to $d_{\text{Ni-S}}\simeq 2.39$ Å in NiS) arises from the fact that S $3p$ orbitals are much more spatially extended in nature than O $2p$ and hence have a larger overlap integral with Ni $3d$ orbitals. In general, Δ is expected to be smaller for sulphides compared to oxides, since the O $2p$ levels are more stable than the S $3p$ levels; for example, the estimated Δ for NiO is 5.5 eV (Ref. 17) compared to 2.5 eV in NiS. The value of U_{dd} for NiS (4.0 eV) is much smaller than that in NiO (6.5 eV) possibly due to a more efficient screening in NiS, arising from the smaller charge transfer energy, Δ and larger hopping strength $(pd\sigma)$, leading to stronger covalency effects.

We have analyzed the ground-state wave function of NiS corresponding to the estimated parameter strengths in terms of the various electron configurations. The ground state of the system was found to consist of 60.7%, 35.8%, and 3.4% of d^8, $d^9\boldsymbol{L}^1$, and $d^{10}\boldsymbol{L}^2$ configurations with a high-spin configuration ($S=1$). The average value of the d-occupancy (n_d) is found to be 8.43, showing a highly covalent ground state of the system. In the case of NiO, a typical divalent oxide of Ni, n_d is found to be ~ 8.16.[17] We have analyzed the characters of the final-states of the system responsible for different features in the experimental spectrum, in order to understand their origins. The analysis was carried out for the final-state energies marked 1–10 in Fig. 4. The different contributions to the final states from various electron configurations (d^8, $d^9\boldsymbol{L}^1$, $d^{10}\boldsymbol{L}^2$) are listed in Table. I. These features can be grouped into three different regions; the main peak region, 852–856 eV (labeled 1–3 in Fig. 4); intense satellite region, 858–861 eV (labeled 4–6), and weak satellites in the region 863–866 eV (labeled 7–10). The first group of features in the main peak region has a dominant $d^9\boldsymbol{L}^1$ character as seen from the table, which are the ''well-screened'' states of the system and correspond to one ligand (sulphur) electron being transferred to the Ni site to screen the Ni $2p$ core-hole potential created by the photoemission process. The second group of features, has a mixed character with significant contributions from all the configurations. This is in contrast to the case of NiO where the intense satellite structure results primarily from the ''poorly-screened'' d^8 configuration. The third group of features has a dominant $d^{10}\boldsymbol{L}^2$ contribution for the lower-energy region (labeled 7 and 8) and a dominant d^8 character for the higher-energy region (labeled 9 and 10 in Fig. 4), with a considerable amount of $d^9\boldsymbol{L}^1$ character for the entire region.

The XP valence-band spectrum of NiS has also been calculated within the same model. An important feature of the present calculation is that the S $3p$ contribution to the VB spectrum has been calculated on the same footing as the contribution from the Ni $3d$ within the *same* model without the need to adjust either the shape or the energy position of the ligand contribution to the valence-band region, thereby enhancing the reliability of the estimated parameter strengths. The calculated spectrum (solid line) along with the Ni $3d$ (dashed line) and S $3p$ (dot-dash line) contributions for NiS are shown superimposed on the experimental data (open circles) in Fig. 5. An inelastic-scattering background function (dotted line) is also included in the total calculated spectrum. The calculated contribution from the Ni $3d$ to the total spectrum for NiS is also shown without any broadening effect as an energy stick diagram in Fig. 5. The parameter set used for the VB calculation is similar to that used for the core-level calculation, but with a Ni $3d$-S $3p$ $(pd\sigma)$ of -1.2 eV instead of -1.4 eV. Such minor adjustments of parameter strengths between the simulations for the core and valence level photoemission spectra, are of common occurrence. The present estimates of the electronic structure parameters are similar to that obtained from the previous valence-band calculations[12] within the cluster model. The agreement between the experimental spectrum and the calculated spectrum in this paper (see Fig. 5) is remarkable over

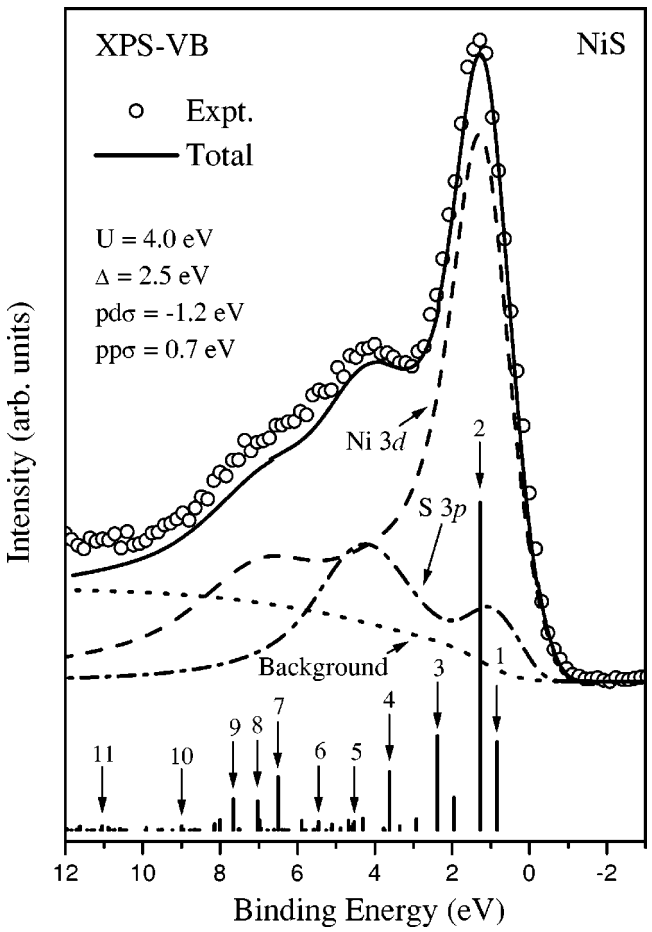

FIG. 5. The experimental VB spectrum (open circles) along with the calculated spectrum (solid line), Ni $3d$ component (dashed line), S $3p$ component (dot-dashed line), and the integral background (dotted line) are shown for NiS. The final states of the calculation and the corresponding intensities without any broadening are shown as the energy stick diagram.

the entire energy range. The main peak in the valence-band spectrum in Fig. 5 at about 1.3 eV arises essentially from Ni $3d$ photoemission contribution, though there is a small contribution arising from S $3p$ states also due to the covalent mixing of states. It is possible to delineate such contributions only in the present approach where S $3p$ contribution is also calculated within the same model. Within the traditional approach, S $3p$ contribution would be approximated by a single Gaussian with its peak position, width, and intensity being freely adjusted to obtain the best possible description. Clearly the present approach is more reliable and satisfactory. A second, and more intense, S $3p$ contribution is responsible for the experimental spectral feature near 4-eV binding energy. The shoulder appearing between about 6 and 9 eV is once again dominated by the Ni $3d$ contributions. This observation along with the fact that this feature is not in agreement with the *ab initio* band-structure results (see Fig. 2), clearly suggests that this feature is driven by correlation effects. The analysis of the ground-state wave function for the parameter set used for the VB spectrum shows that the ground state has 64.9%, 32.6%, and 2.5% of d^8, $d^9\underline{L}^1$, and $d^{10}\underline{L}^2$ characters giving rise to an average d-occupancy (n_d) of 8.38 electrons with a high-spin configuration for the Ni^{2+}, similar to that obtained from the core-level calculation. The parameter strengths estimated here place $NiS_{1-x}Se_x$ samples in the pd-metal region of the ZSA phase diagram.[22,23]

The results of the character analysis of the final states, labeled 1–11 in the figure, corresponding to the Ni $3d$ contribution in the VB spectrum of NiS, are shown in Table. II. On the basis of this analysis, the spectral features can be grouped into three regions, the main peak region (0–6 eV, labeled 1–6 in Fig. 5), the strong satellites in the 6–8.5 eV range (labeled 7–9) and weaker satellites beyond 8.5 eV (marked 10 and 11). The final states in the main peak region predominantly consist of $d^8\underline{L}^1$ states with non-negligible contributions from d^7 and $d^9\underline{L}^2$ configurations. This is similar to the scenario as observered in the case of other charge-transfer systems, like NiO. In the satellite region (6–8.5 eV), the final states are dominated by d^7 and $d^9\underline{L}^2$ configurations. The weak intensity features at higher energies are dominated by $d^9\underline{L}^2$ configuration with a substantial contribution also from $d^8\underline{L}^1$ states. It is to be noted that the first ionization state, marked 1 in the figure, is not at the Fermi energy. This is the well-known artifact of finite cluster-model calculations that invariably exhibit a gap in the charge excitation spectrum due to the discrete eigenspectrum of a finite cluster. It is believed that this ionization state acquires a bandwidth in the thermodynamic limit closing the discrete gap and overlapping the E_F. A dispersion width of less than 1 eV is seen to be sufficient to bring this about; such a dispersion is consistent with our results obtained from LMTO band-structure calculations for the infinite solid. While we have not performed an analysis of the orbital symmetry, our analysis for the first ionization state shows it to be a spin-doublet state.

It is evident that the shoulderlike structure at around 7 eV in the experimental VB spectrum is primarily due to the satellite structure of Ni $3d$ states and is expected to have some nonbonding S $3p$ contribution as seen from its photon energy dependence (see Fig. 3). This explains the inability of

TABLE II. Contributions from various configurations in the final states of the valence-band photoemission in NiS. The peak numberings correspond to the labels indicated in Fig. 5; the corresponding binding energies (BE) in eV are also shown.

Peak no.	1	2	3	4	5	6	7	8	9	10	11
BE	0.8	1.3	2.4	3.6	4.5	5.5	6.5	7.0	7.7	9.0	11.1
d^7	12.23	26.12	15.23	0.00	0.43	1.39	51.91	30.73	44.40	12.22	9.71
$d^8\underline{L}^1$	57.07	57.13	60.15	78.46	72.52	77.24	10.46	19.32	7.64	27.31	36.88
$d^9\underline{L}^2$	28.35	16.16	23.56	21.54	25.98	20.79	34.78	40.57	43.69	60.19	50.48
$d^{10}\underline{L}^3$	2.35	0.59	1.06	0.00	1.07	0.58	2.85	9.38	4.27	0.28	2.93

the band-structure calculations to explain this feature, as the origin of this feature is primarily due to the electron correlations present in the system, giving rise to strong satellite structures. The same correlation effects are also responsible for shifting the main peak to a lower energy and making it narrower compared to the band-structure results (see Fig. 3). This satellite structure, with a dominant d^7 character, is the spectral signature of the lower Hubbard band. This observation along with the highly conducting Pauli paramagnetic property of these compounds suggests that the Hubbard sidebands exist deep inside the metallic regime. This is in accordance with the predictions of the dynamical mean-field theory (DMFT) calculations based on the Hubbard model,[24] that well-defined Hubbard bands continue to exist in the spectral functions even far away from the Mott transition in the metallic region, though the Mott-Hubbard gap collapses by the transfer of spectral weight from the Hubbard sidebands to the coherent spectral features near the E_F region.

In conclusion, we have investigated $NiS_{1-x}Se_x$ using various electron spectroscopic techniques to elucidate the underlying electronic structure. The substitution of Se in place of S does not show appreciable changes in the electronic structure of the system, indicating similar electronic parameters for this solid solution. The band-structure results do not describe well the details of the spectral features in the paramagnetic phase of the system, while a parametrized many-body multiband model is found to be successful in describing the core-level and valence-band spectrum of the NiS. The core-level and valence-band spectral calculations of paramagnetic metallic phase of NiS show that it is a correlated metal with a highly covalent character. The asymmetric line shape as well as the weak feature in the core-level spectra have been ascribed to extrinsic loss processes in the system. The valence-band calculations show that lower Hubbard band exists well inside the pd metallic regime, as predicted by the DMFT calculations. The electronic parameter strengths obtained for the compounds of this solid solution show that they belong to the pd metallic regime of the ZSA phase diagram.

ACKNOWLEDGMENTS

The authors thank Professor C. N. R. Rao for continued support and the Department of Science and Technology, and the Board of Research in Nuclear Sciences, Government of India, for financial support. S.R.K. thanks the Council of Scientific and Industrial Research, Government of India, for financial assistance. D.D.S. thanks Dr. M. Methfessel, Dr. A. T. Paxton, and Dr. M. van Schiljgaarde for making the LMTO-ASA band-structure program available. The authors also thank Professor S. Ramasesha and the Supercomputer Education and Research Center, Indian Institute of Science, for providing the computational facility.

*Also at Jawaharlal Nehru Center for Advanced Scientific Research, Bangalore, India. Electronic address: sarma@sscu.iisc.ernet.in

[1] D.D. Sarma, S.R. Krishnakumar, N. Chandrasekharan, E. Weschke, C. Schüßler-Langeheine, L. Kilian, and G. Kaindl, Phys. Rev. Lett. **80**, 1284 (1998).

[2] M. Nakamura, A. Sekiyama, H. Namatame, H. Kino, A. Fujimori, A. Misu, H. Ikoma, M. Matoba, and S. Anzai, Phys. Rev. Lett. **73**, 2891 (1994).

[3] Richard F. Koehler, Jr. and Robert L. White, J. Appl. Phys. **44**, 1682 (1973).

[4] J.M.D. Coey, R. Brusetti, A. Kallel, J. Schweizer, and H. Fuess, Phys. Rev. Lett. **32**, 1257 (1974).

[5] N. Tsuda, K. Nasu, A. Yanase, and K. Siratori, *Electronic Conduction in Oxides* (Springer-Verlag, Berlin, 1991).

[6] D.B. Mcwhan, M. Marezio, J.P. Remeika, and P.D. Dernier, Phys. Rev. B **5**, 2552 (1972).

[7] S. Anzai, M. Matoba, M. Hatori, and H. Sakamoto, J. Phys. Soc. Jpn. **55**, 2531 (1986).

[8] J. Trahan, R.G. Goodrich, and S.F. Watkins, Phys. Rev. B **2**, 2859 (1970).

[9] L.F. Mattheiss, Phys. Rev. B **10**, 995 (1974).

[10] A. Fujimori, M. Matoba, S. Anzai, K. Terakura, M. Taniguchi, S. Ogawa, and S. Suga, J. Magn. Magn. Mater. **70**, 67 (1987).

[11] P. Raybaud, J. Hafner, G. Kresse, and H. Toulhoat, J. Phys.: Condens. Matter **9**, 11 107 (1997).

[12] A. Fujimori, K. Mamiya, T. Mizokawa, T. Miyadai, T. Sekiguchi, H. Takahashi, N. Mori, and S. Suga, Phys. Rev. B **54**, 16 329 (1996); A. Fujimori, K. Terakura, M. Taniguchi, S. Ogawa, S. Suga, M. Matoba, and S. Anzai, *ibid.* **37**, 3109 (1988).

[13] A.E. Bocquet, T. Mizokawa, A. Fujimori, M. Matoba, and S. Anzai, Phys. Rev. B **52**, 13 838 (1995); A.E. Bocquet, T. Mizokawa, K. Mamiya, A. Fujimori, M. Matoba, S. Anzai, and S. Suga, J. Phys.: Condens. Matter **7**, L411 (1995).

[14] M. Matoba, S. Anzai, and A. Fujimori, J. Phys. Soc. Jpn. **60**, 4230 (1986).

[15] H. Winter, P.J. Durham, and G.M. Stocks, J. Phys. F: Met. Phys. **14**, 1047 (1984).

[16] Priya Mahadevan and D.D. Sarma, Phys. Rev. B **61**, 7402 (2000); Priya Mahadevan, Ph. D. thesis, Department of Physics, Indian Institute of Science, Bangalore, 1998.

[17] K. Maiti, P. Mahadevan, and D.D. Sarma, Phys. Rev. B **59**, 12 457 (1999).

[18] J.C. Slater and G.F. Koster, Phys. Rev. **94**, 1498 (1954).

[19] J.J. Yeh and I. Lindau, At. Data Nucl. Data Tables **32**, 1 (1985).

[20] Unpublished results from the group.

[21] S.R. Barman, A. Chainani, and D.D. Sarma, Phys. Rev. B **49**, 8475 (1994).

[22] J. Zaanen, G.A. Sawatzky, and J.W. Allen, Phys. Rev. Lett. **55**, 418 (1985).

[23] D.D. Sarma, H.R. Krishnamurthy, S. Nimkar, S. Ramasesha, P.P. Mitra, and T.V. Ramakrishnan, Pramana-J. Phys. **38**, L531 (1992); S. Nimkar, D.D. Sarma, H.R. Krishnamurthy, and S. Ramasesha, Phys. Rev. B **48**, 7355 (1993).

[24] A. Georges, and G. Kotliar, Phys. Rev. B **45**, 6479 (1992).